PCCP

Structural and catalytic properties of the Au25-xAgx(SCH3)18 (x = 6, 7, 8) Nanocluster

Journal:	*Physical Chemistry Chemical Physics*
Manuscript ID	CP-ART-10-2017-007295.R3
Article Type:	Paper
Date Submitted by the Author:	29-Apr-2018
Complete List of Authors:	Jin, Rongchao; Carnegie Mellon University, Chemistry Panapitiya, Gihan ; West Virginia University Wang, Hong; West Virginia University, Chen, Yuxiang; Carnegie Mellon Univ, Chem Hussain, Ejaz ; Carnegie Mellon University, Chemistry; Quaid-i-Azam University, Chemistry Lewis, James; West Virginia University,

Structural and catalytic properties of the $Au_{25-x}Ag_x(SCH_3)_{18}$ (x = 6, 7, 8) nanocluster

Gihan Panapitiya[†], Hong Wang[†], Yuxiang Chen[‡], Ejaz Hussain[‡], Rongchao Jin[‡*] and James P. Lewis[†*]

[†]Department of Physics and Astronomy, West Virginia University, Morgantown, WV, 26506-6315

[‡]Department of Chemistry, Carnegie Mellon University, Pittsburgh, PA, 15213

E-mail: james.lewis@mail.wvu.edu, rongchao@andrew.cmu.edu

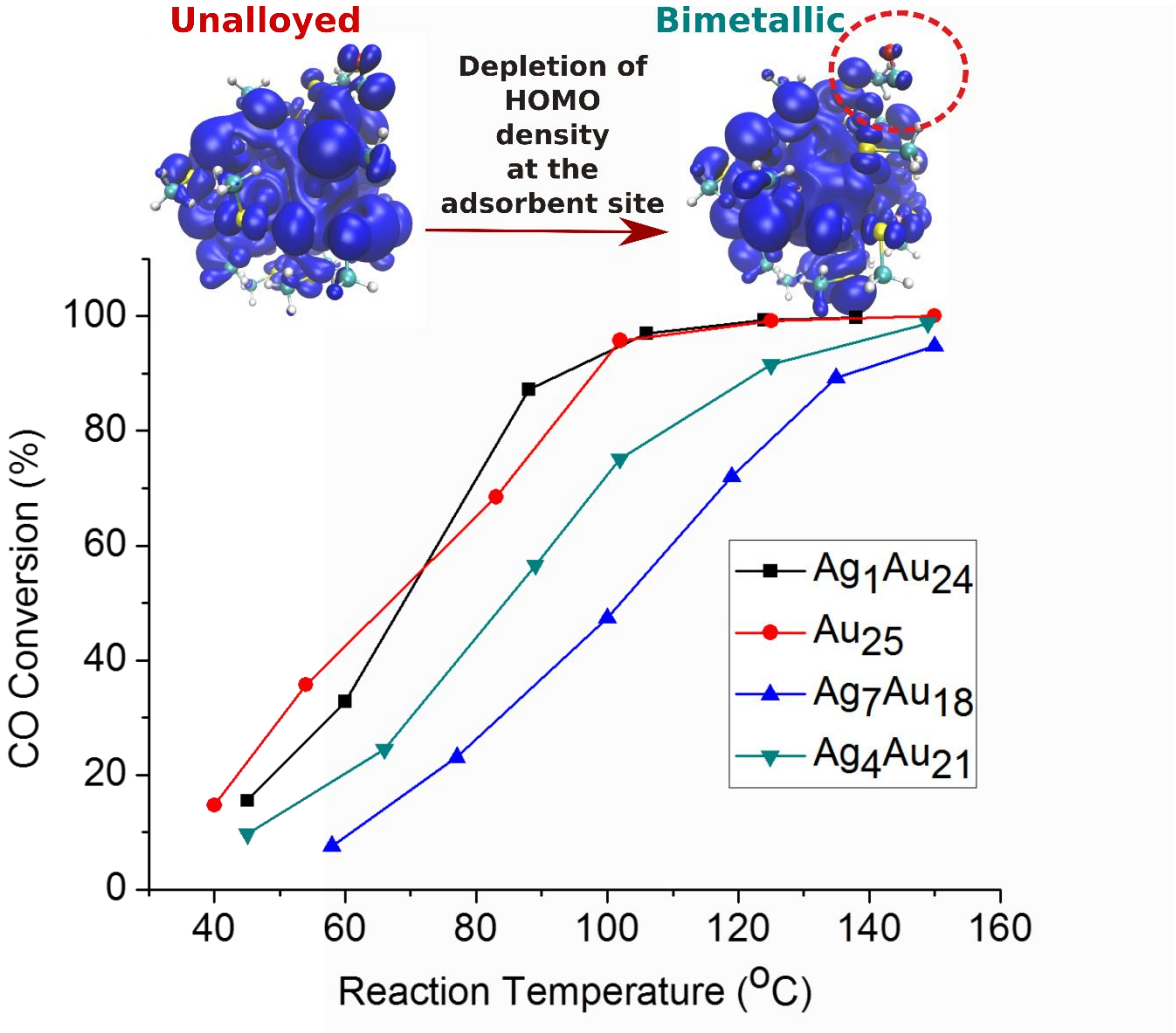

Abstract

In this study, we explore the structural, electronic and catalytic properties of bimetallic nanoparticles of the form $Au_{25-x}Ag_x(SR)_{18}$ (for x = 6,7,8). Due to the combinatorial enormity of the number of different alloyed structures, we choose 500 random configurations corresponding to each alloying level and energetically optimize their structures. Here we report the properties of the lowest energy structures and determine the most favorable Ag alloying sites for these systems. We also show that, nanoalloys with one Ag at the center and the rest in the outer shell of the Au13 kernel are less energetically favorable than the ones with all the Ag atoms occupying the surface of the Au13 kernel. We further present experimental results showing that catalytic oxidation of CO is adversely affected due to Ag alloying. We provide qualitative and quantitative evidence to explain this reduction of the catalytic activity using Fukui functions and average adsorption energies respectively.

Introduction

Thiolate-protected gold nanoclusters, $Au_m(SR)_n$ have attracted scientific attention as novel functional nanomaterials due to their excellent stability [1–8] and unique physical and chemical properties that distinguish them from their bulk counterpart.[9–13] Synthesizing nanoclusters precisely at the atomic level provides a platform to study the fundamental properties of these clusters in depth.[14] $Au_{25}(SR)_{18}$ is one of the widely studied gold nanoclusters that exhibits sizes smaller than 2 nm.[15–20] This nanoparticle has a core-shell structure, in that the core is composed of an Au13 icosahedron surrounded by 12 Au atoms held in staples of SR-Au-SR-Au-SR units.[1,2,21,22] We divide the total 25 Au atoms into three categories, the center Au atom, 12 Au atoms closest to the center atom (which will hereafter be called as the outer shell of the Au13 icosahedron), and the outer shell of remaining 12 Au atoms interacting with the ligands (see Figure 1). All the Au atoms in the outer shell of the Au13 icosahedron and the outer shell are bonded to thiolate ligands. Given this unique structural configuration, the molecular behavior of $Au_{25}(SR)_{18}$ opens up many possibilities to alter the electronic properties considerably by substituting heteroatoms.[23–26]

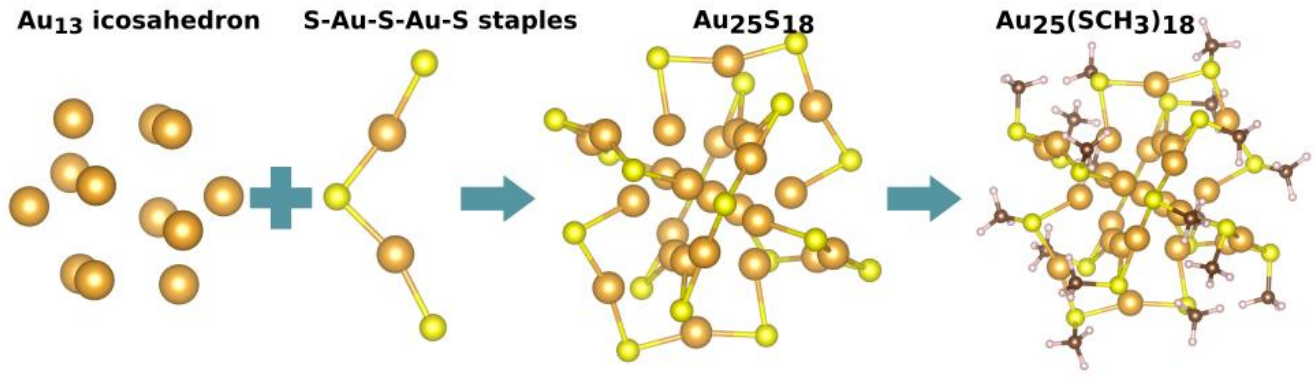

Figure 1 schematic of the $Au_{25}(SCH_3)_{18}$ nanocluster (orange, Au; yellow,S; brown, C; pink, H).

A single substitution of a heteroatom can significantly change the electronic structure and chemical properties in $Au_{25}(SR)_{18}$. [27–29,24] Jiang and Dai have proposed 16 elements as candidates for doping the Au25 cluster such that the electronic and the geometric structure of the unalloyed system are maintained.[28] Several groups have been successful in increasing the number of dopants in the cluster. [30,17] These reports show that the maximum Ag incorporation can be up to 12 silver atoms.

A study by Walter and Moseler proposed that the preferential occupying positions of Ag should occur in the Au13 icosahedral core.[31] This result was also confirmed by later studies of Guidez et al., Gottlieb et al and Tlahuice-Flores. [3,17,32] A study by Kumara et al. showed using x-ray crystallographic data, that the central Au atom of Au13 core is exclusively an Au domain while the remainder of the Au13 icosahedron is partially occupied by Au or Ag atoms.[33] Recent work by Jin et al demonstrated that it is also possible to dope the staple sites by increasing the number of Ag atoms up to 19.[34]

A study by Negishi et al. found that the electronic structure of $(AuAg)_{25}(SR)_{18}$ can be continuously modulated by the incorporation of up to 11 Ag atoms.[30] They demonstrated that alloying Ag was possibly an effective method to tune the electronic structures and physical properties. Kauffman et al. have investigated $Au_{25-x}Ag_x(SR)_{18}$, where x = 0 to 5 and R = C_2H_4Ph, combining both experimental and computational studies. [35] They have observed that a mixing between Au and Ag electronic states perturbs discrete energy levels, which leads to a shift of the optical absorption peak and introduce new features into the $Au_{25-x}Ag_x$ absorption spectrum. Kumara et al. have also shown that the optical absorption peaks shift to higher energies in Au25 nanocluster due to Ag alloying.[33] This result has been reproduced computationally by Tlahuice-Flores who further shows that the peak corresponding to the HOMO-LUMO gap shifts to lower energies in alloyed clusters where the number of Ag atoms is greater than 12.[32]

Several groups report on the catalytic activity of pure $Au_{25}(SR)_{18}$ system. [36–39] Jin et al. have found that Au3 sites in $Au_{25}(SR)_{18}$ are the most reactive ones and demonstrated that with R = CH_2CH_2Ph, this nanocluster supported on oxides can catalyze Sonogashira cross-coupling reaction between phenylacetylene and p-iodoanisole with high conversion of p-iodoanisole.

[36,40] Using DFT methods, Jiang et al. have presented a possible mechanism for the selective hydrogenation of *α,β*-unsaturated ketones to unsaturated alcohols on the $Au_{25}(SR)_{18}$ cluster.[38] Li and Jin al have investigated the catalytic properties of $Ag_xAu_{25-x}(SR)_{18}$ and $Cu_xAu_{25-x}(SR)_{18}$ based on the selective oxidation of styrene to styrene epoxide and benzaldihyde. They have found that the inner shell of MAu affects the selectivities for the main products.[41] Li et al. have compared the catalytic activity of titania-supported $Au_{25}(SR)_{18}$ and $M_xAu_{25-x}(SR)_{18}$ (M = Pt,Cu, Ag) and found that $Au_{25}(SR)_{18}$ performed better than the other bimetalic clustes.[42] The catalytic activity of M_xAu(M = Au,Cu,Ag) supported on CeO_2 has been shown to decrease in the order $Cu_xAu_{25-x}(SC_2H_4Ph)_{18}$ > $Au_{25}(SC_2H_4Ph)_{18}$ > $Ag_xAu_{25-x}(SC_2H_4Ph)_{18}$, based on the CO conversion to CO_2 by Li et al. Their DFT calculations indicates that adsorption energy of CO on the nanocluster follow the same trend as that of the reactivity.[43]

Even though the size of Au25 nanocluster is quite accessible for the general DFT computational techniques, it is still challenging to determine the doping sites and geometric structures once the doping number increases beyond x=4.

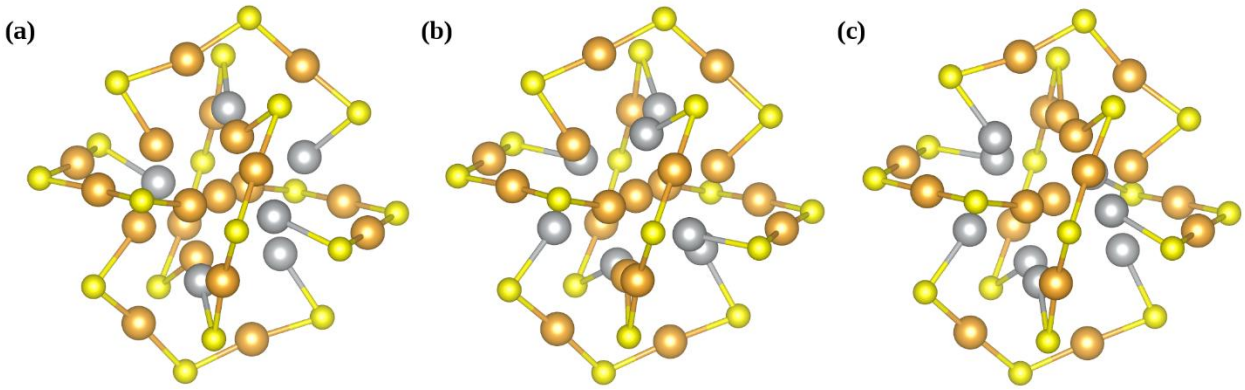

Figure 2 Lowest energy isomers of (a) 6-, (b) 7- and (c) 8-Ag alloyed clusters (grey, Ag).

Although experimental work has mapped out the preferred Ag doping sites to be on the icosahedral shell, the partial occupancy in X-ray analysis only gave an averaged result which did not tell the specific configuration of dopants, for example, whether the Ag dopants would be clustering together or maximally isolated.

Herein, we combine both experimental and computational research to identify the preferred doping locations of Ag heteroatom substitutions in the $Au_{25-x}Ag_x(SR)_{18}$ cluster with x = 6,7,8. Figure 2 shows the lowest energy isomers for each alloying level considered in this work. We find that due to the Ag dopants, 2-fold and 3-fold symmetries displayed by the unalloyed cluster are broken in these lowest energy structures. As depicted in supplementary Figure S16, only remaining symmetry is the reflection symmetry in 7- and 8-Ag alloyed lowest energy isomers.

Mass spectrometry has detected $Au_{19}Ag_6$, $Au_{18}Ag_7$, and $Au_{17}Ag_8$ as the most abundant species in a sample where doping number(x) can vary between 5 and 9. Although the spectrometric signal of $Au_{18}Ag_7$ seems to be dominant than the other two, we still cannot neglect the effect from $Au_{19}Ag_6$ and $Au_{17}Ag_8$ species in the sample. Accordingly, we propose to analyze the electronic properties using weighted average density of states in order to account for the presence of all the alloyed species indicated in the mass spectrum. We also suggest to employ Fukui functions as a qualitative descriptor of catalytic activity together with traditional quantitative descriptors like adsorption energies.

Experimental

Synthesis and Methodologies

The synthetic details of $Au_{25}(SC_2H_4Ph)_{18}$ and $Ag_xAu_{25-x}(SC_2H_4Ph)_{18}$ nanoclusters can be found in references 17 and 23 , respectively. $Ag_xAu_{25}(SC_2H_4Ph)_{18}$ (x = 0-9) nanoclusters were deposited onto CeO_2 powders (200 mg) by wet deposition.[44] After stirring for 24 h, all the nanoclusters were adsorbed onto CeO_2 support, as the supernatant became colorless. The as-prepared catalysts were dried at ambient temperature and no further treatment was performed unless otherwise noted.

100 mg of $Ag_xAu_{25-x}(SC_2H_4Ph)_{18}$ (x = 0-9)/CeO_2 was mixed with quartz wool and tested for CO oxidation in a fixed-bed, continuous flow reactor (8 mm i.d.) under ambient pressure.[45] Before CO oxidation test, the as-prepared catalysts were pretreated at 150°C in diluted O_2 (O_2/He = 10/90 volume) for 1 h and then cooled down to room temperature. The reaction gas mixture of 3% CO, 10% O_2 and 87% He flowed through the reaction bed at a flow rate of 40 ml min^{-1}. The reaction products were analyzed by an online gas chromatograph (HP 6890) equipped with a carbon molecular sieve column and a thermal conductivity detector.

Matrix-assisted laser desorption ionization (MALDI) mass spectrometry was performed with a PerSeptive-Biosystems Voyager DE super-STR time-of-flight (TOF) mass spectrometer. Trans-2-[3-(4-tert-Butylphenyl)-2-methyl-2-propenyldidene] malononitrile (DCTB) was used as the matrix. Typically, 0.5 mg of matrix and 0.005 mg of $Ag_xAu_{25-x}(SC_2H_4Ph)_{18}$ nanocluster (i.e., a 100:1 mass ratio between DCTB and sample) were mixed in 50 μL of CH_2Cl_2. A 10 μL portion of solution was applied to the steel plate and air-dried.

Computational Tools

The starting point of our computational procedure is to choose an optimal $Au_{25}(SR)_{18}$ structure, which possesses the geometric and chemical features similar to that of the actual experimentally synthesized $Au_{25}(SC_2H_4Ph)_{18}$ nanocluster. We adopted the previously studied geometry of $Au_{25}(SH)_{18}$ and replaced the -SH with $-SCH_3$ group to mimic the $-SC_2H_4Ph$ ligand.[35] To validate our computational approach, we have tested the $Au_{25-x}Ag_x$ (x = 1 to 3) cases as

discussed in the supporting Information. For the case of $Au_{22}Ag_3$, there are 2300 confirmations examined and analyzed, including the symmetry equivalent and inequivalent doping sites. We identified that the outer shell of the Au13 icosahedron served as the energetically favorable sites for 3 Ag heteroatoms substitution, agreeing with the previous studies.[35] The same computational procedure was applied to study Ag alloying levels with Au:Ag ratios of 19:6, 18:7 and 17:8. Figure 2 shows the lowest energy structures of Ag substituted isomers at random Au sites according to these ratios.

All the calculations are carried out using FIREBALL, an open source DFT package which is based on the density functional theory, implemented within a nonlocal pseudo-potential scheme. [46,47] Two types of exchange-correlation density functionals are available with FIREBALL, LDA and GGA (BLYP).[48,47] Within the LDA, the exchange-correlation is designed to exactly reproduce the energy and potential of the uniform electronic structures. On the other hand, the Becke exchange with Lee-Yang-Parr correlation functional (BLYP) is known to provide reasonably good energy values for metal containing systems and high levels of accuracy in the determination of a geometry optimization. [49] In our study, the geometric structures and energies are of primary focus. Thus, (BLYP) exchange was used. As for the basis set, we chose the optimized numerical local atomic orbitals. These orbital wavefunctions have a cutoff radii *Rc*, beyond which the wavefunctions vanish. The single numerical (SN) basis set was selected for H element with R_c values, $R_c^H(s)$ = 4.1 a.u. and the double numerical (DN) basis set was selected for C, O and S elements with R_c values, $R_c^C(s)$ = 4.3 a.u, $R_c^C(p)$ = 4.7 a.u, $R_c^O(s)$= 3.6 a.u, $R_c^O(p)$ = 4.0 a.u, $R_c^S(s)$ = 4.5 a.u, $R_c^S(p)$ = 5.0 a.u. For the metal elements (Ag and Au), we used the polarized basis set sp^3d^5 by adding a p orbital to the minimal basis set sd^5. The cutoff radii were $R_c^{Ag}(s)$ = 5.6 a.u, $R_c^{Ag}(p)$ = 5.9 a.u, $R_c^{Ag}(d)$ = 4.9 a.u; $R_c^{Au}(s)$ = 5.4 a.u, $R_c^{Au}(p)$ = 5.8 a.u, $R_c^{Au}(d)$ = 5.0 a.u. Catalytic reactivity of Au nanocatalysts is examined using the Fukui functions. The frontier orbital (FO) theory proposed by Fukui provides a general qualitative approach to understand and interpret the chemical reactions. [50,51] FO theory considers the distribution of electron densities of the frontier orbitals as the principle factor to reveal the conceptual behavior of a molecule in the presence of an approaching reagent. Parr and Yang have rationalized the features of the frontier orbital theory within the density functional theory by using a finite difference approximation. They have defined the Fukui function as the response in the density function $\rho(r)$ to a change in the number of electrons (N) in the system, under constant external potential $v(r)$, $f(r) = \left[\frac{\partial \rho(r)}{\partial N}\right]_{v(r)}$. [52–54] There are three types of Fukui Functions given by, $f^-(r)$, $f^+(r)$ and $f^0(r)$ corresponding to the electrophilic, nucleophilic, and radical attack respectively.

$$f^-(r) = \rho_{N_0 0}(r) - \rho_{N_0 - 1}(r) \approx \rho_{HOMO}$$
$$f^+(r) = \rho_{N_0 + 1}(r) - \rho_{N_0 0}(r) \approx \rho_{LUMO} \quad (1)$$

Here, N_0 is the number of electrons in the system. ρ_{HOMO} and ρ_{LUMO} correspond to the ground state electron densities of the highest occupied molecular orbital (HOMO) and lowest unoccupied molecular orbital (LUMO) respectively.

Results and Discussion

The composition of $Au_{25-x}Ag$(SR) nanoclusters (from low silver content to moderate then to high silver content) was determined by matrix-assisted laser desorption ionization mass spectroscopy (MALDI-MS), as shown in Figure 3a. Each peak corresponds to a specific number of silver atoms doped into the Au25 framework, as labeled on the top of the Figure 3a; for example, x = 1 indicates a single silver atom incorporated into the Au25 framework and results in the $AgAu_{24}$ nanoalloy. The intensity of the peak in MALDI-MS corresponds to the relative abundance of each species, which depends on the reaction time. The longer the reaction time the larger is the number of Ag atoms corresponding to the dominant peak in the mass spectrum. [17]

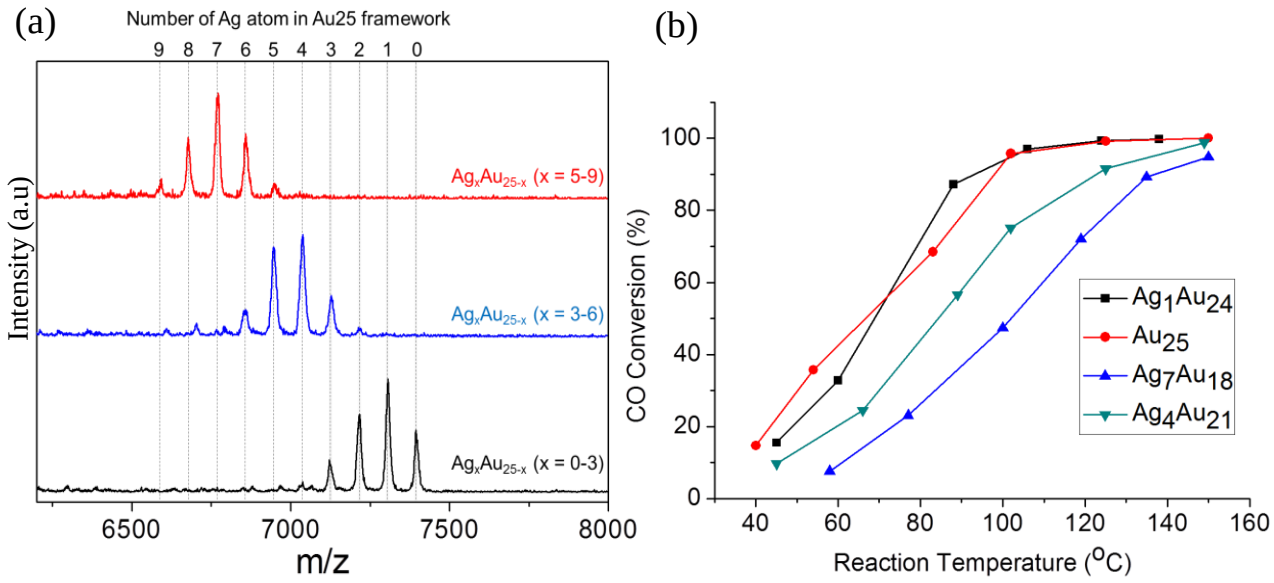

Figure 3 (a) MALDI-MS of $Au_{25-x}Ag_x(SR)_{18}$ nanoalloys. (b) Temperature dependent CO conversion rates)

This ability to synthesize bimetallic nanoparticles immediately invites a study on their performance as catalysts as Ag possesses favorable catalytic properties. In particular, we find that the CO oxidation reaction is significantly affected by the Ag alloying. As shown in Figure 3b, the percentage of CO converted to CO_2 in the reaction temperature range 40 - 160 °C, decreases with the increasing number of Ag atoms in the nanoparticle, indicating a reduction in the catalytic activity. Investigating the factors that affect the catalytic activity, as the number of Ag atoms varies in the nanoparticle, is experimentally challenging as it requires the synthesis of atomically precise Ag alloyed nanoparticles. However, the current synthesis procedures result

in a mixture of alloyed species of $Au_{25-x}Ag_x$ with x having a range of values as depicted in Figure 3a.

To obtain a clear picture of the alloyed structures and dopant impacts, our simulations focused on studying the individual alloying levels (x = 6, 7 and 8) of $Au_{25-x}Ag_x(SCH_3)_{18}$ clusters. We used 500 symmetry inequivalent and equivalent structures with Ag atoms substituted at random Au sites for each alloying level in high-throughput calculations, with exhaustive search for energetically favorable nanoparticles. We optimized all these structures until the root-mean-square of the force on the atoms falls below 0.05 eV/Å. Supporting Information section contains detailed results of these calculations which are consistent with a previous study on the substitution of three Ag atoms.[35] Figure 4 presents our results on the structural analysis of the three sampling populations. It is evident that the energetically favorable confirmations are the ones with a majority of the Ag atoms in the outer shell of the Au13 icosahedron of the nanoparticle. To further confirm this trend, we created another sampling pool of 50 structures for each alloying level, and confined Ag atoms only to the Au13 icosahedron. In this case also, the Ag sites in the outer shell of the Au13 icosahedron have been selected randomly. We analyzed the structural trends of the 10 lowest energy structures from each sampling set containing 50 structures (golden bars in Figure 4(b), (d) and (f)), and found that the structures with all the Ag atoms in the outer shell of the Au13 icosahedron are indeed more energetically favorable. Figure S17 shows Boltzmann distributions for all the 550 isomers considered in this study for each alloying level. The molecular structures of ten of the lowest energy isomers for each alloying level are given in the supporting information (Figures S11-S13). It is also interesting to note that the structures with one Ag atom at the center and the rest in the outer shell of the Au13 icosahedron is at least 0.7 eV higher than the lowest energy isomer (with all the Ag atoms in the outer shell of the Au13 icosahedron). A silver atom at the center results in a larger number adjacent Ag atoms with respect to the case when Ag is not in the center. In this regard, Ag atoms clustered at close proximities to each other seems to be less energetically favorable. This observation is similar what has been reported by Guidez et al.[3] Although, we identified the outer shell of the Au13 icosahedron as the preferred sites, this does not overrule the possibility for one or two Ag atoms going to the other locations. However, the majority of Ag atoms will go to the sites in the outer shell of the Au13 icosahedron.

One important feature of the gold clusters is the molecular-like electronic properties, which distinct them from their bulk counterpart. Jin and coworkers have shown that both HOMO and LUMO of $Au_{25}(SR_3)_{18}$ are mainly contributed by the gold 6p , 5d and sulfur 3p orbitals (see Figure S2) and HOMO level is triply degenerate and LUMO level doubly degenerate.[2]

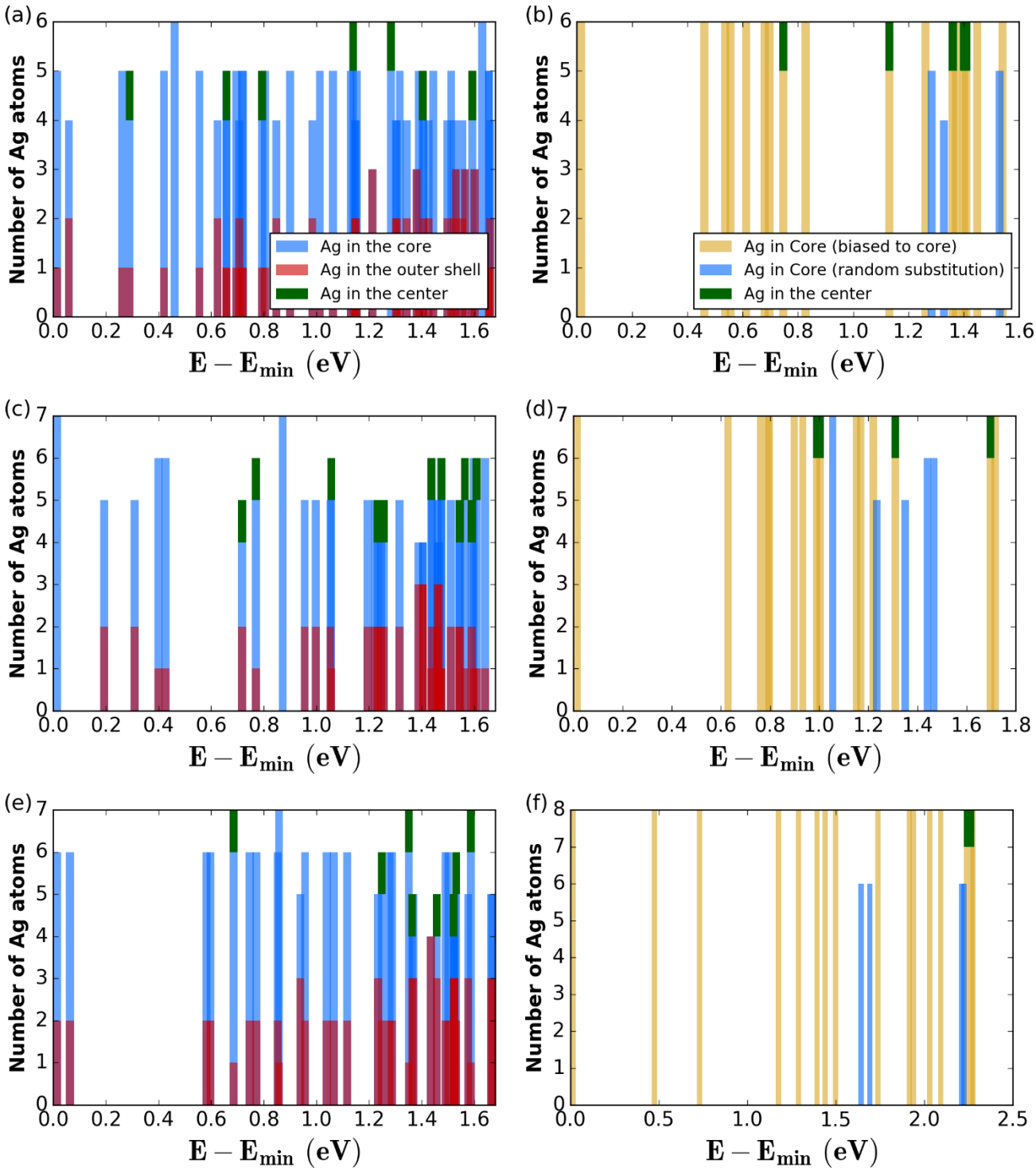

Figure 4 Structural trends of (a) 6-, (c) 7- and (e) 8-Ag alloyed nanoclusters (only 50 lowest energy structures are shown for clarity). Blue and red color bars correspond to the cases where Ag atoms are in the outer shell of the Au13 icosahedron and outer shell respectively. Gold bars in (b), (d) and (f) correspond to the structures with Ag atoms biased exclusively to the Au13 icosahedron for, 6-, 7- and 8-Ag alloying levels respectively. Blue bars in (b), (d) and (f) correspond to the randomly substituted lowest energy structures of (a), (b) and (c) respectively. Dark green bars correspond to the cases where the substituted site is the center atom of Au13 icosahedron. In the legends, "random substitution" refers to randomly selecting Ag alloying sites and "biased to core" refers to restricting the Ag substitution only to the Au13 icosahedron.

Majority of HOMO and LUMO states are localized at the central Au13 kernel (see Figure S4). Due to the fact that the energetically favorable alloying sites for Ag have been identified as the outer shell of the Au13 icosahedron, major changes in the frontier orbital states can be expected when compared with the unalloyed structure. The HOMO-LUMO energy gap for the charge-neutral $Au_{25-x}Ag_x(SCH_3)_{18}$ is about 1.36 eV, which is comparable to the experimental absorption band at 670 nm reported by Jin et al. [55]

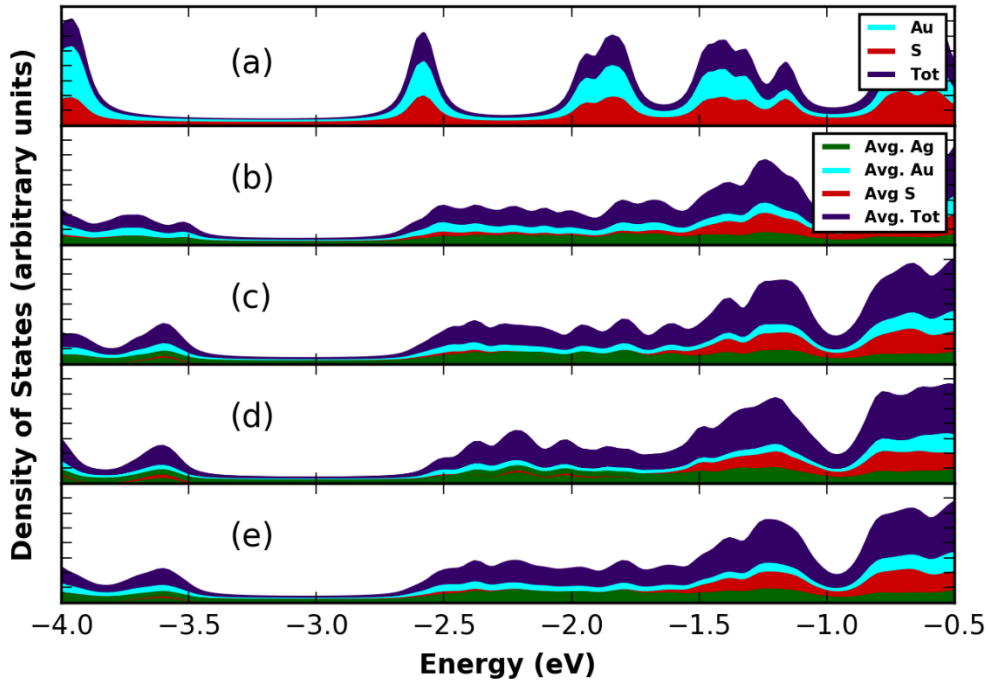

Figure 5 Density of states (DOS) and partial density of states (PDOS) for (a) 0-, (b) 6-,(c) 7- and (e) 8-Ag alloyed nanoclusters in comparison with the (e) weighted average DOS and PDOS over 6,7, and 8-Ag cases.(Weights are based on the height of the peaks in the MALDI-MS)

Previously published experimental work on the Ag alloying in Au25 shows that the photon absorption energy increases with the increasing number of Ag atoms in the cluster.[30] These experimental data also shows a significant broadening in the absorption peaks at the vicinity of the main absorption peak in the Ag alloyed structures. Our density of states (DOS) results, shown in Figure 5, are in agreement with this observation. In Figure 5(e), we present the weighted average DOS, of which the weights reflect the relative abundance of each Ag alloyed species, which is given by the peaks in the mass spectrum. In the un-alloyed structure, there are two sharp peaks in the DOS, corresponding to the HOMO and LUMO levels (Figure 5 (a)) and a region without any states immediately after the LUMO level. This absence of states can limit electron transitions at these energies, resulting in very low absorption intensities. This feature is absent in the Ag alloyed structures. Instead of a single dominant peak, LUMO level is composed of a broadened region of many electronic states in the alloyed nanoparticles. This availability of more LUMO states enables higher energy HOMO-LUMO transitions than the ones allowed in the un-alloyed structure. Due to this, the average photon absorption energy can

increase, creating a peak at a higher energy value in the photon absorption spectrum for Ag alloyed structures. A closer look at the DOS reveals that this broadening is mediated mainly by the newly formed silver S states (Figure S3). As the number of Ag atoms increases, the number of these S states at the LUMO level also increases, thereby amplifying the broadening. The weighted average DOS (Figure 5 (e)) further confirms the emergence of new states between -2.5 and -2.0 eV as an effect coming from the LUMO electronic states in 6-, 7- and 8-Ag alloyed nanoparticles. To explain the trend in the CO conversion rates (see Figure 3b) in the Ag alloyed systems, we studied HOMO, LUMO densities and CO adsorption energies of CO adsorbed $Au_{25-x}Ag_x(SCH_3)_{18}$. The main purpose of this study is to understand the interaction between CO and Au25 cluster and how Ag alloying affects it. We note that in practice, several CO and O_2 molecules get adsorbed on the nanocluster. This introduces additional, more complex interactions (CO-CO, O_2-O_2, CO-O_2) which hinders the understanding about how each reactant interacts with Au25. Therefore as a starting point we considered the interaction between CO and Au25. CO was placed near a particular Au/Ag atom in the ten lowest energy isomers chosen from the pools of 550 randomly substituted Au25 clusters for each alloying level. All these CO adsorbed isomers were optimized prior to calculating the electron densities and the adsorption energies. Adsorption energy was calculated as,

$$E_{Au25+CO} - (E_{Au25} + E_{CO}) \qquad (2),$$

where $E_{Au25+CO}$ is the energy of the composite Au25+CO system after adsorption and E_{Au25} and E_{CO} are the energies of Au25 and CO molecules respectively. Thus, the greater the negative value of the adsorption energy, the stronger is the adsorption. Average adsorption energies over 10 lowest energy structures are shown in Figure 6. Different colors of the bars correspond to the cases where CO is placed near different Au/Ag sites in the outer shell (Figure S15). Structural energies of all the structures considered in Figure 6 are given in Figure S18. Out of the nanoclusters considered in the current study, CO binding is strongest in the nanoalloys with 6 Ag atoms. This result contradicts with the general trend for catalytic activity shown in Figure 3b, which is that the catalytic activity reduces with the increasing number of Ag dopants. However, according to Figure 3a, the synthesis of 7-Ag alloyed nanoclusters results in a mixture of structures containing 6- and 8-Ag alloyed species with relative abundances of 25% and 24% respectively. 7-Ag structures account for 41% of the total number of structures in the experimental mixture (Figure 3a). Thus, the reduced catalytic activity observed for 7-Ag nanoalloys (Figure 3b) can be mainly attributed to the lower adsorption energies of 7- and 8-Ag alloyed clusters which constitute about 65% of the synthesized nanoalloys. We also calculted the adsorption energies of the nanocluster with all the Au sites replaced with Ag. We found that these energies greater than those of the other alloyed systems considered in this work. This trend shows that the reactivity of the Ag alloyed nanoclusters decreases with the increasing number of the Ag atoms.

Experimentally, it is not possible to control the number CO molecules interacting with Au25. Therefore, it is interesting to study how CO-CO interaction energy affects the adsorption energy. By considering two CO molecules adsorbed on nearest neighbor Au/Ag sites, we find that the CO-CO interaction slightly increases the adsorption energy of the two-CO-adsorbed isomers (Figure S20, Table S1). In other words, the interaction between CO molecules weakens the adhession of CO on Au25 cluser. We also notice that the interaction energy is largest in 6-Ag alloyed isomers. However, the trend in the adsorption energies are similar to that with one CO molecule. Therefore in the following discusion we only consider one CO adsorbed isomers.

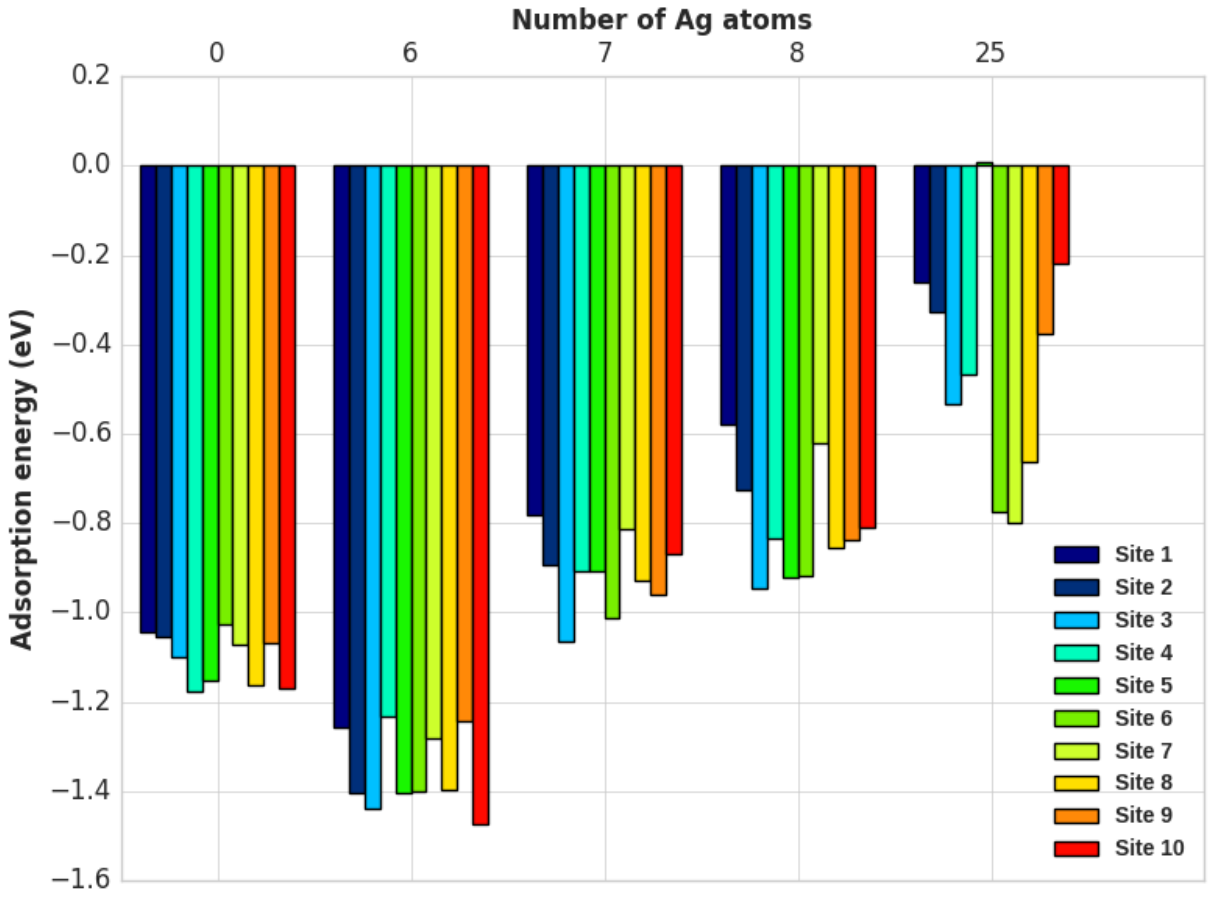

Figure 6 Average CO adsorption energies of the nanoalloys. Different colored bars refer to 10 different Au/Ag CO adsorption sites in the outer shell.

To get a further qualitative insight on that catalytic activity of these Ag alloyed nanoclusters, we analyzed the electron densities of the frontier molecular orbitals, HOMO and LUMO. We observed that for 0-Ag structure, LUMO density near CO is denser than the corresponding HOMO density (Figure 7a and b). According to the definitions of the Fukui functions, this shows that CO tends to attract electrons in the vicinity of Au25. For effective charge transfer between CO and the outer shell atoms of the nanocluster, the Ag/Au atoms near CO should

be willing to donate electrons. That is, the HOMO densities at Ag/Au atoms should be substantial. When the HOMO densities of low energy 6-, 7- and 8-Ag alloyed structures are examined, we see that these HOMO densities are considerably low for majority of the structures (Figure 7c-7e, S5-S7). Even though there are a small number of structures for which this argument does not hold, we note that the electronic properties of a mixture of alloyed structures with different energies are dictated by the dominant electronic features. We also find that the HOMO and LUMO densities of 25-Ag alloyed system are comparable with the 6, 7 and 8-Ag alloyed systems as shown Figure S19, agreeing with the relationship between the adsorption energy and Fukui functions as discussed above.

We also note that ligands used in experimental synthesis of Au25 are bigger than –SCH3

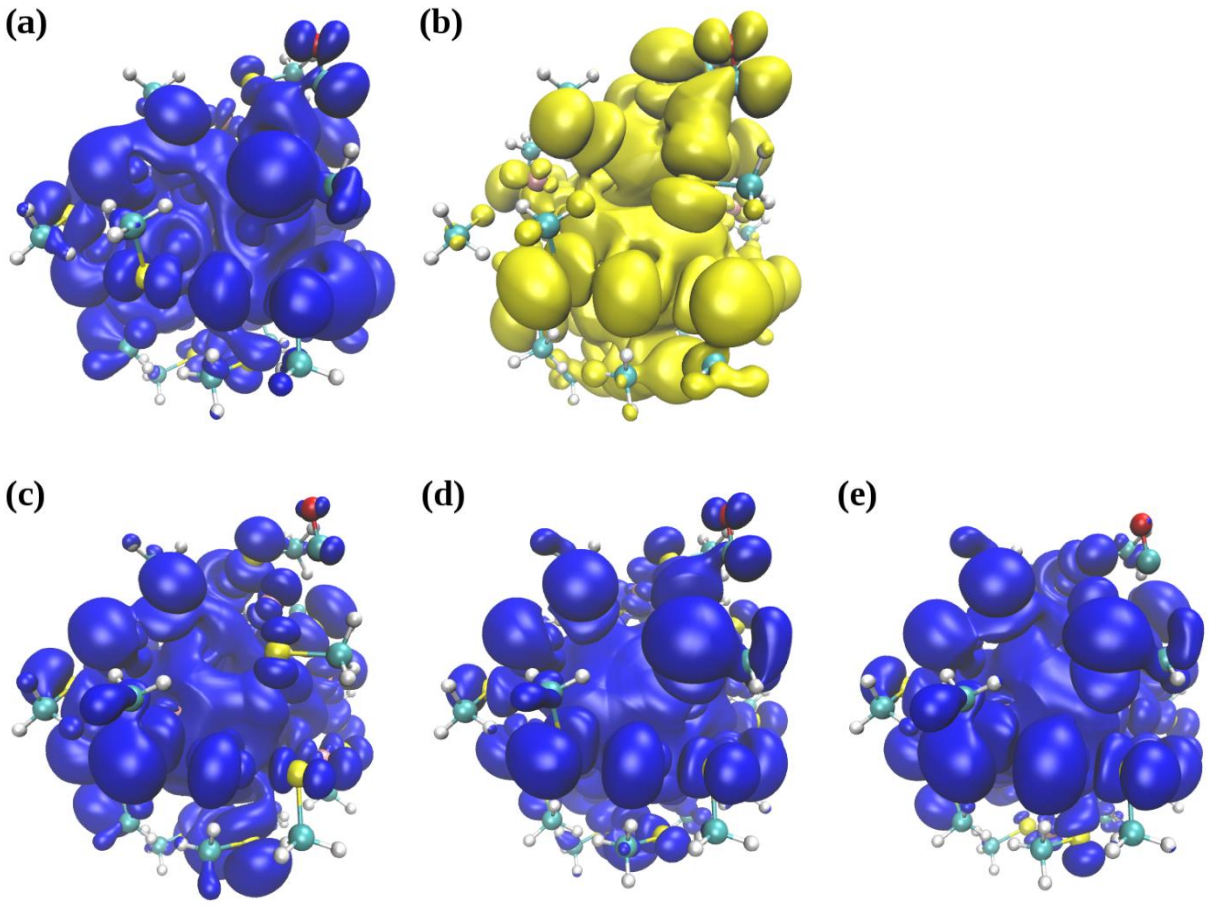

Figure 7 (a) HOMO and (b) LUMO electron densities of unalloyed Au25 nanoculster. HOMO electron densities of (c) 6- , (d) 7- and (e) 8-Ag alloyed nanoclusters (isovalue = 0.0002)

Reduction in the HOMO density of the reactive Ag/Au atom can also be examined using density of states plots. In Figure 8a and 8b we show the average DOS of the adsorbent Au/Ag atom and the adsorbate C atom of the ten lowest energy structures respectively. Even though there is a drop in the number of both HOMO and LUMO states contributed

by the Au atom in the alloyed systems compared to the unalloyed one, the reduction in the HOMO states is greater than that of the LUMO states. This indicates that the electron donating capability of Au/Ag is more adversely affected than its electron attracting strength. In fact, according to the Fukui theory, Ag alloying has switched the role of this Au/Ag atom from being a charge donor to a charge accepter. The electron attracting nature of the C atom on the other hand is less affected due to the presence of Ag (Figure 8b) given by its dominant LUMO density. We think that this tendency to attract electrons by both Au and adsorbate C reduces the adsorption strength between CO and Au/Ag sites, which adversely affects the catalytic activity of CO oxidation.

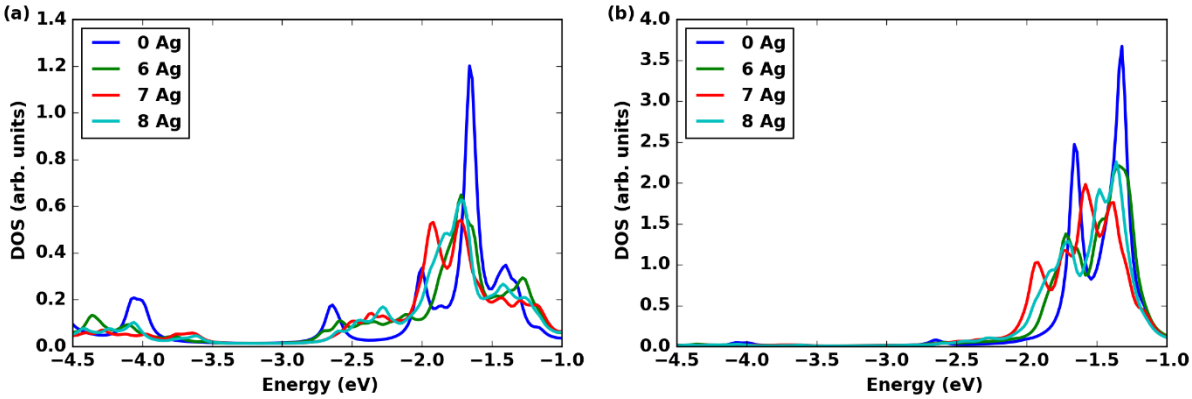

Figure 8 Average PDOS of (a) Au atom at the adsorbent site and (b) C atom of CO

In order to check whether this model based on the adsorption energies and Fukui functions generalize for other adsorbed systems, we considered the adsorption of styrene molecule on Au25. We chose styrene because Liu et al. have demonstrated that Au25 supported on hydroxyapatite act as an effective catalyst for styrene epoxidation.[11] Styrene is considerably larger than CO. Its' adsorption cannot be tested on individual Ag/Au sites as we have done for CO. Therefore we considered 8 triangular facets as the adsorption sites, as shown in Figure 9. Due to the steric hindrance from the -SCH3 ligands not all the facets are equally approachable for styrene. Therefore we considered one of the facets with the least hindrance for this analysis. The adsorption energies and the HOMO and LUMO densities are shown Figure 9. We found that the adsorption energies follow the trend observed for the CO adsorption. However we could not establish a solid correlation between the Fukui functions and the adsorption energies apart from the fact that the nucleophilic attack Fukui function values are larger in Ag alloyed structures when compared with the unalloyed one. Due to the larger size of the styrene molecule, its adsorption on Au25 depends on many interactions mainly with three -SCH3 ligands as well as the three Ag/Au atoms in the considered facet. Because of this, we believe that Fukui functions cannot be used as the sole descriptor to explain the changes in the adsorption energies in the case of styrene adsorption.

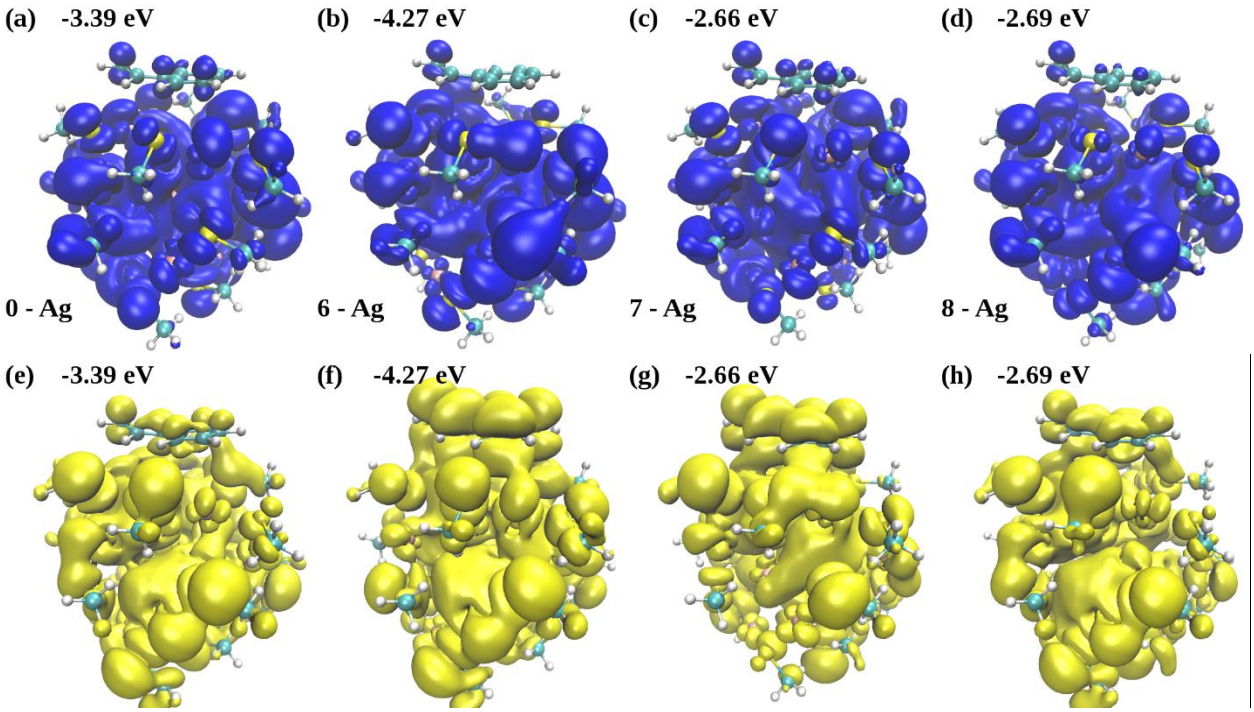

Figure 9 HOMO (a-d) and LUMO (e-f) electron densities of styrene adsorbed 0-, 6- , 7- and 8-Ag alloyed nanoclusters. Adsorption energies are given next to the image label.

Conclusion

In summary, we studied the structural, electronic and catalytic properties of 6, 7 and 8 Ag alloyed $Au_{25}(SR)_{18}$ nanocluster using both experimental and computational techniques. We found that all the Ag atoms occupying the outer shell of the Au13 icosahedron results in the most energetically favorable bimetallic structures. The HOMO-LUMO gaps in the Ag alloyed nanoparticles reduce by about 0.5 eV compared to the unalloyed structure. This reduction does not contradict with the observed increase in the absorption energies as the number of Ag atoms increases. Our DOS calculations show that the presence of broadened LUMO electronic states in the alloyed systems can enhance optical absorption across the HOMO-LUMO gap. Adsorption energies of 7- and 8-Ag alloyed clusters are significantly lower than that of the non-alloyed structure. According to Fukui theory, depleted HOMO densities at the Au/Ag sites in the alloyed systems indicate that electron donating capability of the adsorbent sites reduces in alloyed systems. These theoretical observations quantitatively and qualitatively explain the reduced catalytic activity of $Au_{25-x}Ag_x$ nanoalloys in terms of the changes introduced by Ag in the electronic structure of the Au25 cluster. We also find that adsorption energies for styrene also followed the same trend observed for CO. However, due to the complex interactions between styrene and Au25 these trends cannot be explained based on the Fukui functions only.

Acknowledgement

This work is supported by the National Science Foundation (DMREF CHE-1434378) and the Department of Energy (DE-SC0004737, DE-SC0014429).

Supporting Information Available

Structural trends of $[Au_{22}Ag_3(SCH_3)_{18}]^0$, $[Au_{22}Ag_3(SH)_{18}]^0$ and $[Au_{22}Ag_3(SH)_{18}]^{-1}$ (Figure S1); Partial DOS of 0, 3, 6, 7, 8-Ag alloyed Au25 clusters (Figure S2 and Figure S3); HOMO and LUMO molecular orbitals and electron densities of non-alloyed and alloyed Au25 cluster (Figure S4-S10); Structures of lowest energy isomers (Figure S11-S13); Bond lengths obtained with BLYP functional (Figure S14); Different Ag/Au sites considered for CO adsorption (Figure S15); Symmetries displayed by the lowest energy alloyed isomers (Figure S16); Boltzmann distributions of all the isomers (Figure S17); Energies of CO adsorbed isomers (Figure S18); HOMO and LUMO densities of Ag25 (Figure S19); Weighted average adsorption energies of Au25/2CO systems (Figure S20, Table S1); Atomic coordinates of the lowest energy alloyed isomers; Adsorption energies of all the sites in the Au25/CO system (Figure S21).

References

(1) Heaven, M. W.; Dass, A.; White, P. S.; Holt, K. M.; Murray, R. W. Crystal Structure of the Gold Nanoparticle $[N(C_8H_{17})_4][Au_{25}(SCH_2CH_2Ph)_{18}]$. *J. Am. Chem. Soc.* **2008**, *130* (12), 3754–3755.

(2) Zhu, M.; Aikens, C. M.; Hollander, F. J.; Schatz, G. C.; Jin, R. Correlating the Crystal Structure of a Thiol-Protected Au_{25} Cluster and Optical Properties. *J. Am. Chem. Soc.* **2008**, *130* (18), 5883–5885.

(3) Guidez, E. B.; Mäkinen, V.; Häkkinen, H.; Aikens, C. M. Effects of Silver Doping on the Geometric and Electronic Structure and Optical Absorption Spectra of the $Au_{25-n}Ag_n(SH)_{18}^-$(N = 1, 2, 4, 6, 8, 10, 12) Bimetallic Nanoclusters. *J. Phys. Chem. C* **2012**, *116* (38), 20617–20624.

(4) Tsukuda, T. Toward an Atomic-Level Understanding of Size-Specific Properties of Protected and Stabilized Gold Clusters. *Bull. Chem. Soc. Jpn.* **2012**, *85* (2), 151–168.

(5) Tlahuice, A.; Garzón, I. L. On the Structure of the $Au_{18}(SR)_{14}$ Cluster. *Phys. Chem. Chem. Phys.* **2012**, *14* (11), 3737–3740.

(6) Negishi, Y. Toward the Creation of Functionalized Metal Nanoclusters and Highly Active Photocatalytic Materials Using Thiolate-Protected Magic Gold Clusters. *Bull. Chem. Soc. Jpn.* **2014**, *87* (3), 375–389.

(7) Xu, W. W.; Zhu, B.; Zeng, X. C.; Gao, Y. A Grand Unified Model for Liganded Gold Clusters. *Nat. Commun.* **2016**, *7*, 13574.

(8) Jin, R.; Zeng, C.; Zhou, M.; Chen, Y. Atomically Precise Colloidal Metal Nanoclusters and Nanoparticles: Fundamentals and Opportunities. *Chem. Rev.* **2016**, *116* (18), 10346–10413.

(9) Jin, R.; Charles Cao, Y.; Hao, E.; Metraux, G. S.; Schatz, G. C.; Mirkin, C. A. Controlling Anisotropic Nanoparticle Growth through Plasmon Excitation. *Nature* **2003**, *425* (6957), 487–490.

(10) Rosi, N. L.; Mirkin, C. A. Nanostructures in Biodiagnostics. *Chem. Rev.* **2005**, *105* (4), 1547–1562.

(11) Liu, Y.; Tsunoyama, H.; Akita, T.; Tsukuda, T. Efficient and Selective Epoxidation of Styrene with TBHP Catalyzed by Au_{25} Clusters on Hydroxyapatite. *Chem. Commun.* **2010**, *46* (4), 550–552.

(12) Li, G.; Jin, R. Atomically Precise Gold Nanoclusters as New Model Catalysts. *Acc. Chem. Res.* **2013**, *46* (8), 1749–1758.

(13) Yang, S.; Wang, S.; Jin, S.; Chen, S.; Sheng, H.; Zhu, M. A Metal Exchange Method for Thiolate-Protected Tri-Metal $M_1Ag_xAu_{24-x}(SR)_{18}^0$ (M = Cd/Hg) Nanoclusters. *Nanoscale* **2015**, *7* (22), 10005–10007.

(14) Jin, R.; Nobusada, K. Doping and Alloying in Atomically Precise Gold Nanoparticles. *Nano Res.* **2014**, *7* (3), 285–300.

(15) Parker, J. F.; Fields-Zinna, C. A.; Murray, R. W. The Story of a Monodisperse Gold Nanoparticle: $Au_{25}L_{18}$. *Acc. Chem. Res.* **2010**, *43* (9), 1289–1296.

(16) MacDonald, M. A.; Chevrier, D. M.; Zhang, P.; Qian, H.; Jin, R. The Structure and Bonding of $Au_{25}(SR)_{18}$ Nanoclusters from EXAFS: The Interplay of Metallic and Molecular Behavior. *J. Phys. Chem. C* **2011**, *115* (31), 15282–15287.

(17) Gottlieb, E.; Qian, H.; Jin, R. Atomic-Level Alloying and de-Alloying in Doped Gold Nanoparticles. *Chemistry* **2013**, *19* (13), 4238–4243.

(18) Antonello, S.; Perera, N. V; Ruzzi, M.; Gascón, J. A.; Maran, F. Interplay of Charge State, Lability, and Magnetism in the Molecule-like $Au_{25}(SR)_{18}$ Cluster. *J. Am. Chem. Soc.* **2013**, *135* (41), 15585–15594.

(19) De Nardi, M.; Antonello, S.; Jiang, D.; Pan, F.; Rissanen, K.; Ruzzi, M.; Venzo, A.; Zoleo, A.; Maran, F. Gold Nanowired: A Linear $(Au_{25})_n$ Polymer from Au_{25} Molecular Clusters. *ACS Nano* **2014**, *8* (8), 8505–8512.

(20) Yao, C.; Lin, Y.; Yuan, J.; Liao, L.; Zhu, M.; Weng, L.; Yang, J.; Wu, Z. Mono-Cadmium vs Mono-Mercury Doping of Au_{25} Nanoclusters. *J. Am. Chem. Soc.* **2015**, *137* (49), 15350–15353.

(21) Akola, J.; Walter, M.; Whetten, R. L.; Häkkinen, H.; Grönbeck, H. On the Structure of Thiolate-Protected Au_{25}. *J. Am. Chem. Soc.* **2008**, *130* (12), 3756–3757.

(22) Pei, Y.; Zeng, X. C. Investigating the Structural Evolution of Thiolate Protected Gold Clusters from First-Principles. *Nanoscale* **2012**, *4* (14), 4054–4072.

(23) Qian, H.; Jiang, D.; Li, G.; Gayathri, C.; Das, A.; Gil, R. R.; Jin, R. Monoplatinum Doping of Gold Nanoclusters and Catalytic Application. *J. Am. Chem. Soc.* **2012**, *134* (39), 16159–16162.

(24) Christensen, S. L.; MacDonald, M. A.; Chatt, A.; Zhang, P.; Qian, H.; Jin, R. Dopant Location, Local Structure, and Electronic Properties of $Au_{24}Pt(SR)_{18}$ Nanoclusters. *J. Phys. Chem. C* **2012**, *116* (51), 26932–26937.

(25) Yamazoe, S.; Kurashige, W.; Nobusada, K.; Negishi, Y.; Tsukuda, T. Preferential Location of Coinage Metal Dopants (M = Ag or Cu) in $[Au_{25-x}M_x(SC_2H_4Ph)_{18}]^-$ ($X \sim 1$) As Determined by Extended X-Ray Absorption Fine Structure and Density Functional Theory Calc. *J. Phys. Chem. C* **2014**, *118* (43), 25284–25290.

(26) Tian, S.; Liao, L.; Yuan, J.; Yao, C.; Chen, J.; Yang, J.; Wu, Z. Structures and Magnetism of Mono-Palladium and Mono-Platinum Doped $Au_{25}(PET)_{18}$ Nanoclusters. *Chem. Commun.* **2016**, *52* (64), 9873–9876.

(27) Fields-Zinna, C. A.; Crowe, M. C.; Dass, A.; Weaver, J. E. F.; Murray, R. W. Mass Spectrometry of Small Bimetal Monolayer-Protected Clusters. *Langmuir* **2009**, *25* (13), 7704–7710.

(28) Jiang, D.; Dai, S. From Superatomic $Au_{25}(SR)_{18}^-$ to Superatomic $M@Au_{24}(SR)_{18}^q$ Core−Shell Clusters. *Inorg. Chem.* **2009**, *48* (7), 2720–2722.

(29) Miller, S. A.; Fields-Zinna, C. A.; Murray, R. W.; Moran, A. M. Nonlinear Optical Signatures of Core and Ligand Electronic States in $Au_{24}PdL_{18}$. *J. Phys. Chem. Lett.* **2010**, *1* (9), 1383–1387.

(30) Negishi, Y.; Iwai, T.; Ide, M. Continuous Modulation of Electronic Structure of Stable Thiolate-Protected Au_{25} Cluster by Ag Doping. *Chem. Commun.* **2010**, *46* (26), 4713–4715.

(31) Walter, M.; Moseler, M. Ligand-Protected Gold Alloy Clusters: Doping the Superatom. *J. Phys. Chem. C* **2009**, *113* (36), 15834–15837.

(32) Tlahuice-Flores, A. Optical Properties of Thiolate-Protected $Ag_nAu_{25-n}(SCH_3)_{18}^-$ Clusters. *J. Nanoparticle Res.* **2013**, *15* (7), 1771.

(33) Kumara, C.; Aikens, C. M.; Dass, A. X-Ray Crystal Structure and Theoretical Analysis of $Au_{25-x}Ag_x(SCH_2CH_2Ph)_{18}^-$ Alloy. *J. Phys. Chem. Lett.* **2014**, *5* (3), 461–466.

(34) Li, Q.; Wang, S.; Kirschbaum, K.; Lambright, K. J.; Das, A.; Jin, R. Heavily Doped $Au_{25-x}Ag_x(SC_6H_{11})_{18}^-$ Nanoclusters: Silver Goes from the Core to the Surface. *Chem. Commun.* **2016**, *52* (29), 5194–5197.

(35) Kauffman, D. R.; Alfonso, D.; Matranga, C.; Qian, H.; Jin, R. A Quantum Alloy: The Ligand-Protected $Au_{25-x}Ag_x(SR)_{18}$ Cluster. *J. Phys. Chem. C* **2013**, *117* (15), 7914–7923.

(36) Li, G.; Jiang, D.; Liu, C.; Yu, C.; Jin, R. Oxide-Supported Atomically Precise Gold

Nanocluster for Catalyzing Sonogashira Cross-Coupling. *J. Catal.* **2013**, *306*, 177–183.

(37) Li, G.; Jiang, D.; Kumar, S.; Chen, Y.; Jin, R. Size Dependence of Atomically Precise Gold Nanoclusters in Chemoselective Hydrogenation and Active Site Structure. *ACS Catal.* **2014**, *4* (8), 2463–2469.

(38) Ouyang, R.; Jiang, D. Understanding Selective Hydrogenation of A,β-Unsaturated Ketones to Unsaturated Alcohols on the $Au_{25}(SR)_{18}$ Cluster. *ACS Catal.* **2015**, *5* (11), 6624–6629.

(39) Li, G.; Abroshan, H.; Chen, Y.; Jin, R.; Kim, H. J. Experimental and Mechanistic Understanding of Aldehyde Hydrogenation Using Au25 Nanoclusters with Lewis Acids: Unique Sites for Catalytic Reactions. *J. Am. Chem. Soc.* **2015**, *137* (45), 14295–14304.

(40) Li, G.; Jin, R. Gold Nanocluster-Catalyzed Semihydrogenation: A Unique Activation Pathway for Terminal Alkynes. *J. Am. Chem. Soc.* **2014**, *136* (32), 11347–11354.

(41) Li, G.; Jin, R. Atomic Level Tuning of the Catalytic Properties: Doping Effects of 25-Atom Bimetallic Nanoclusters on Styrene Oxidation. *Catal. Today* **2016**, *278*, 187–191.

(42) Li, Z.; Yang, X.; Liu, C.; Wang, J.; Li, G. Effects of Doping in 25-Atom Bimetallic Nanocluster Catalysts for Carbon–carbon Coupling Reaction of Iodoanisole and Phenylacetylene. *Prog. Nat. Sci. Mater. Int.* **2016**, *26* (5), 477–482.

(43) Li, W.; Liu, C.; Abroshan, H.; Ge, Q.; Yang, X.; Xu, H.; Li, G. Catalytic CO Oxidation Using Bimetallic M_xAu_{25-X} Clusters: A Combined Experimental and Computational Study on Doping Effects. *J. Phys. Chem. C* **2016**, *120* (19), 10261–10267.

(44) Nie, X.; Qian, H.; Ge, Q.; Xu, H.; Jin, R. CO Oxidation Catalyzed by Oxide-Supported $Au_{25}(SR)_{18}$ Nanoclusters and Identification of Perimeter Sites as Active Centers. *ACS Nano* **2012**, *6* (7), 6014–6022.

(45) Li, W.; Ge, Q.; Ma, X.; Chen, Y.; Zhu, M.; Xu, H.; Jin, R. Mild Activation of CeO_2 -Supported Gold Nanoclusters and Insight into the Catalytic Behavior in CO Oxidation. *Nanoscale* **2016**, *8* (4), 2378–2385.

(46) Keith, J. B.; Fennick, J. R.; Junkermeier, C. E.; Nelson, D. R.; Lewis, J. P. A Web-Deployed Interface for Performing Ab Initio Molecular Dynamics, Optimization, and Electronic Structure in Fireball. *Comput. Phys. Commun.* **2009**, *180* (3), 418–426.

(47) Lewis, J. P.; Jelínek, P.; Ortega, J.; Demkov, A. A.; Trabada, D. G.; Haycock, B.; Wang, H. H.; Adams, G.; Tomfohr, J. K.; Abad, E.; et al. Advances and Applications in the FIREBALL Ab Initio Tight-Binding Molecular-Dynamics Formalism. *Phys. status solidi* **2011**, *248* (9), 1989–2007.

(48) Jelínek, P.; Wang, H.; Lewis, J. P.; Sankey, O. F.; Ortega, J. Multicenter Approach to the Exchange-Correlation Interactions in *Ab Initio* Tight-Binding Methods. *Phys. Rev. B* **2005**, *71* (23), 235101.

(49) Henrik Grönbeck; Alessandro Curioni, A.; Andreoni, W. Thiols and Disulfides on the Au(111) Surface: The Headgroup−Gold Interaction. *J. Am. Chem. Soc.* **2000**, *122* (16), 3839–3842.

(50) Fukui, K.; Yonezawa, T.; Shingu, H. A Molecular Orbital Theory of Reactivity in Aromatic Hydrocarbons. *J. Chem. Phys.* **1952**, *20* (4), 722–725.

(51) Fukui, K.; Yonezawa, T.; Nagata, C.; Shingu, H. Molecular Orbital Theory of Orientation in Aromatic, Heteroaromatic, and Other Conjugated Molecules. *J. Chem. Phys.* **1954**, *22* (8), 1433–1442.

(52) Yang, W.; Parr, R. G. Hardness, Softness, and the Fukui Function in the Electronic Theory of Metals and Catalysis. *Proc. Natl. Acad. Sci. U. S. A.* **1985**, *82* (20), 6723–6726.

(53) Parr, R. G.; Weitao, Y. *Density-Functional Theory of Atoms and Molecules*; International Series of Monographs on Chemistry; Oxford University Press, 1994.

(54) Kohn, W.; A. D. Becke, A.; Parr, R. G. Density Functional Theory of Electronic Structure. **1996**, *100* (31), 12974–12980.

(55) Zhu, M.; Eckenhoff, W. T.; Pintauer, T.; Jin, R. Conversion of Anionic $[Au_{25}(SCH_2CH_2Ph)_{18}]^-$ Cluster to Charge Neutral Cluster via Air Oxidation. *J. Phys. Chem. C* **2008**, *112* (37), 14221–14224.